

## **Process analytical technology (PAT) applied to biomass valorisation: a kinetic study on the multiphase dehydration of xylose to furfural**

T. Eifert, M. A. Liauw\*

Institut für Technische und Makromolekulare Chemie, RWTH Aachen University, Worringerweg 1, 52074 Aachen, Germany. \*E-Mail: liauw@itmc.rwth-aachen.de, Tel: +49 (0) 241 80 26470

### **Content**

1. Conversion, yield and selectivity of xylose dehydration	2
2. Spectroscopic feasibility	3
3. HPLC, GC and NMR examples	7
4. Raman spectra over the course of the reaction	9
5. Chemometric peak integration models	10
6. Sensitivity analysis	12

## 1. Conversion, yield and selectivity of xylose dehydration

Conversion, yield and selectivity were investigated using offline analytics. Xylose and furfural content in the aqueous phase were determined by HPLC and furfural content in the 2-MTHF phase was determined using GC. Yield and selectivity towards furfural refers to the initial amount of xylose and the final amount of furfural in the entire system.

**Table 1:** Conversion, yield and selectivity of xylose dehydration at different temperatures.

$T/^\circ\text{C}$	$t/\text{h}$	$X_{\text{Xylose}}/\text{mol}\%$	$Y_{\text{Furfural, Xylose}}/\text{mol}\%$	$S_{\text{Furfural}}/\text{mol}\%$
120	5.87	20	9	45
130	5.60	39	29	74
130	5.50	40	21	51
140	3.33	52	27	51
140	1.80	41	20	50
140	0.98	31	9	28
140	0.55	13	6	44
140	0.28	21	2	12
140	2.17	43	22	50
140	4.17	61	44	72
150	3.08	79	42	53
150	2.72	72	37	52
160	1.52	84	38	45

## 2. Spectroscopic feasibility

The analysed peaks and bands need to be originated by the vibrational and electronical excitations of the molecules of interest. The peaks should also rather not overlap completely to allow chemometric evaluation of the spectra.

Due to low concentrations of furfural in the aqueous phase during the reaction, furfural could be quantitatively detected only in the 2-MTHF phase. Humins are crosslinked polymers consisting of furan moieties that are mostly insoluble in both aqueous and organic phases and tend to stick to surfaces. Because of the small spectroscopic penetration depths of the ATR UV/Vis probes and the strong absorption of light in the UV/Vis range due to humins on the surface of the internal reflection element (IRE, a sapphire in this case), furfural could not be analysed by ATR UV/Vis spectroscopy. Furthermore, humins were formed while furfural was produced, thus the humin signal was superimposed on the furfural band in the UV/Vis range. During the reaction, furfural could be detected by ATR mid-IR (Figure 1) and Raman (Figure 2) spectroscopy, because their higher penetration depth leads to a significantly smaller effect of the humin formation on the spectra. Xylose was analysed by ATR mid-IR (Figure 4) and Raman (Figure 3) spectroscopy in the aqueous phase.

To obtain bonding information from the measured spectra, a mid-IR spectrum from xylose in water was calculated by DFT (Figure 5). With the theoretical spectrum it was possible to display the vibrations that led to the specific absorption peaks. Therefore, the analysed peaks from the experimental signal of xylose in the mid-IR fingerprint area between 1000 – 1200  $\text{cm}^{-1}$  were assigned to the calculated peaks which were shifted to higher wavenumbers by ca. 150  $\text{cm}^{-1}$  (see Table 2).

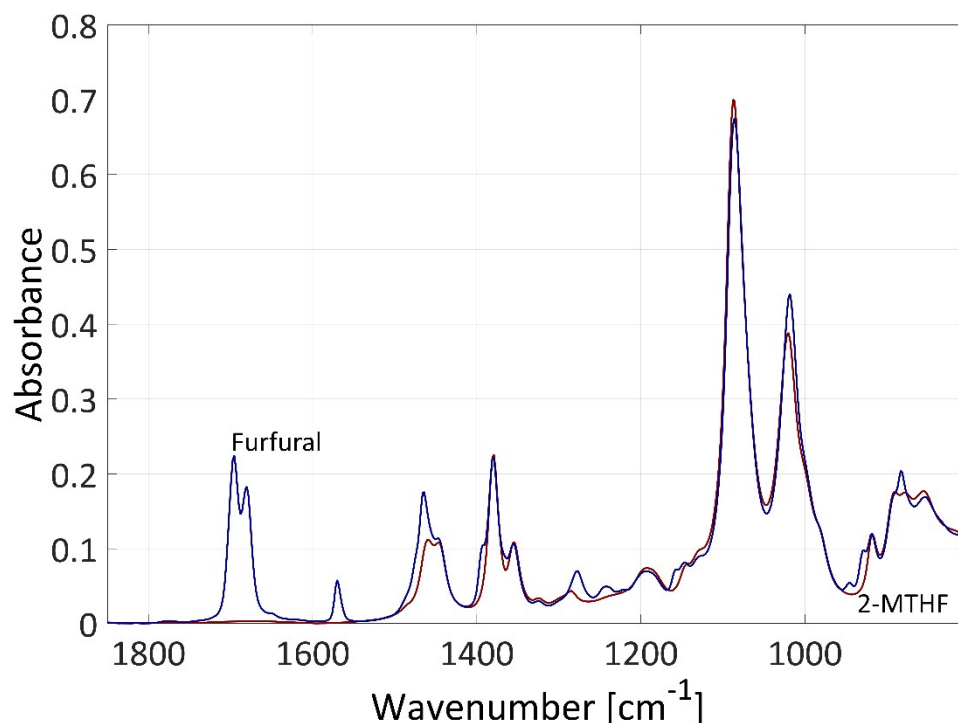


**Figure 1:** ATR mid-IR spectra of 2-MTHF (red, room temperature) and furfural in 2-MTHF (blue,  $c = 1.1 \text{ mol L}^{-1}$ , room temperature). Qualitative accuracy was assured by comparison with literature.<sup>1</sup>

<sup>1</sup> [http://sdbs.db.aist.go.jp/sdbs/cgi-bin/direct\\_frame\\_disp.cgi?sdbno=130](http://sdbs.db.aist.go.jp/sdbs/cgi-bin/direct_frame_disp.cgi?sdbno=130) (National Institute of Advanced Industrial Science and Technology, 11 April 2016)

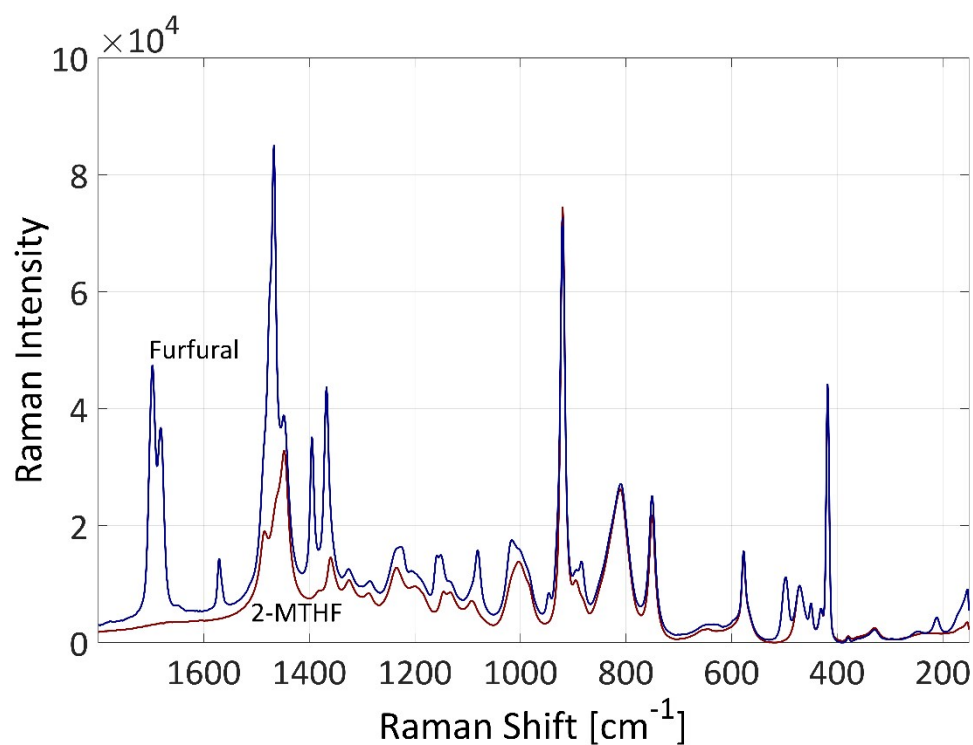


**Figure 2:** Raman spectra of 2-MTHF (red) and furfural in 2-MTHF (blue,  $c = 1.1 \text{ mol L}^{-1}$ , room temperature). Qualitative accuracy was assured by comparison with literature.<sup>2</sup>

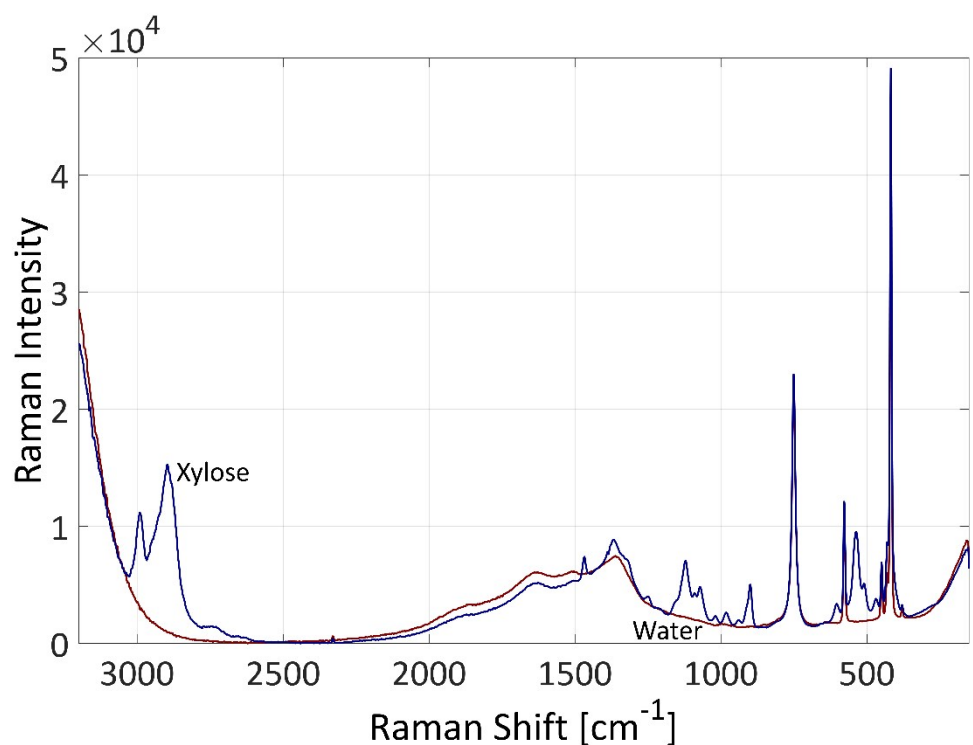


**Figure 3:** Raman spectra of water (red) and xylose in water (blue,  $c = 1.7 \text{ mol L}^{-1}$ , room temperature). Qualitative accuracy was assured by comparison with literature.<sup>3</sup>

<sup>2</sup> T. S. Little, J. Qiu and J. R. Durig, *Spectrochim Acta A*, 1989, **45**, 789-794.

<sup>3</sup> M. F. Mrozek and M. J. Weaver, *Anal Chem*, 2002, **74**, 4069-4075.

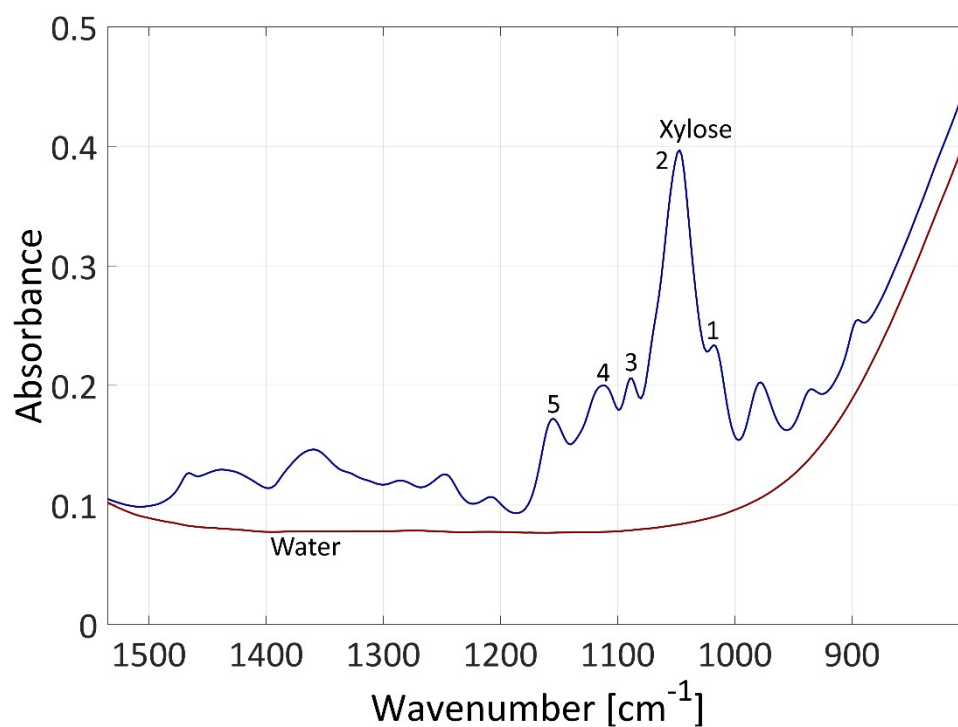


**Figure 4:** ATR mid-IR spectra of water (red) and xylose in water (blue,  $c = 1.7 \text{ mol L}^{-1}$ , room temperature). Qualitative accuracy was assured by comparison with literature.<sup>4</sup>

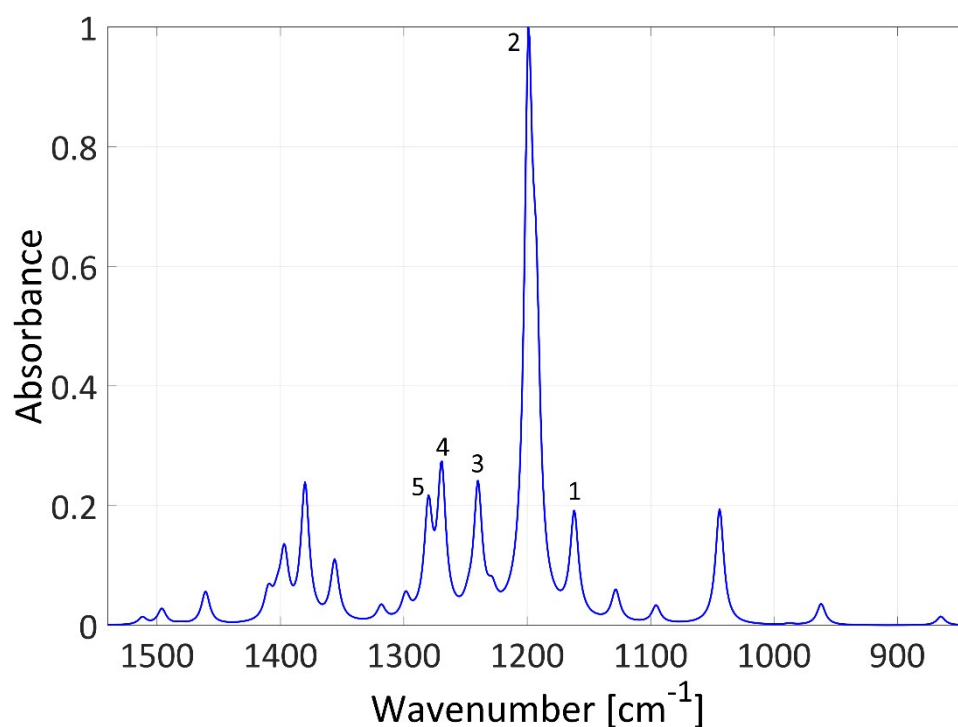


**Figure 5:** DFT calculated mid-IR spectra of xylose with a water shell<sup>5</sup> to extract bonding information from the experimental measured spectra of xylose in water (compare to Figure 4).

<sup>4</sup> [http://sdbs.db.aist.go.jp/sdbs/cgi-bin/direct\\_frame\\_disp.cgi?sdbno=1100](http://sdbs.db.aist.go.jp/sdbs/cgi-bin/direct_frame_disp.cgi?sdbno=1100) (National Institute of Advanced Industrial Science and Technology, 11 April 2016)

<sup>5</sup> Gaussian09, MN12SX/def2-TZVP, SMD solvation model

**Table 2:** Assignment of the experimental peaks of xylose in the mid-IR fingerprint area between 1000 – 1200 cm<sup>-1</sup> to the calculated peaks

Peak #	$\tilde{\nu}$ (ATR mid-IR) /cm <sup>-1</sup>	$\tilde{\nu}$ (DFT) /cm <sup>-1</sup>	Bonding information
1	1018	1162	$\nu$ (C-OH), $\delta$ (R-C-H), $\delta$ (R-O-H), weak
2	1047	1199	$\nu$ (C-O-C), $\delta$ (R-C-H), $\delta$ (R-O-H), strong
3	1088	1240	$\nu$ (C-OH), $\delta$ (R-C-H), $\delta$ (R-O-H), weak
4	1113	1269	$\nu$ (C-OH), $\delta$ (R-C-H), medium
5	1155	1280	$\nu$ (C-OH), $\delta$ (R-C-H), medium

### 3. HPLC, GC and NMR examples

Offline analytics of an aqueous phase after the reaction:

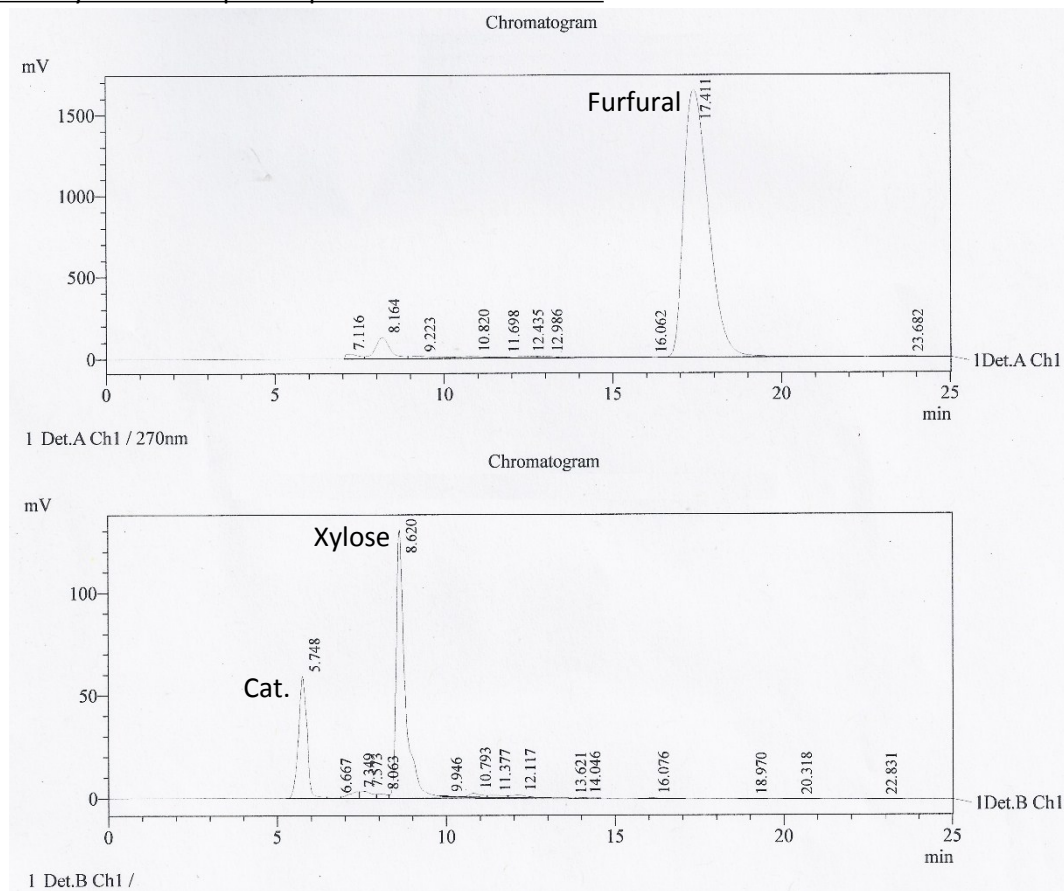


Figure 6: HPLC of a xylose dehydration to furfural at  $T = 140^{\circ}\text{C}$  ( $t = 4$  h).

Offline analytics of a 2-MTHF phase after the reaction:

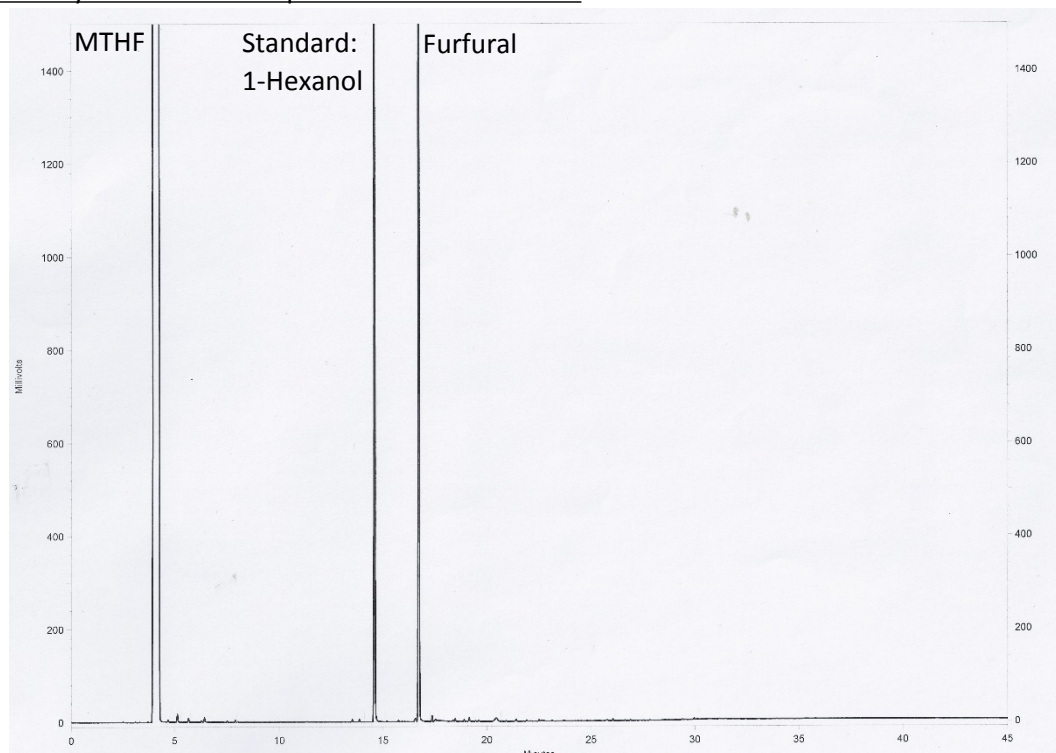


Figure 7: GC of a xylose dehydration to furfural at  $T = 140^{\circ}\text{C}$  ( $t = 4$  h).

NMR spectra of a 2-MTHF phase isolated by distillation in  $\text{CDCl}_3$  after the reaction:

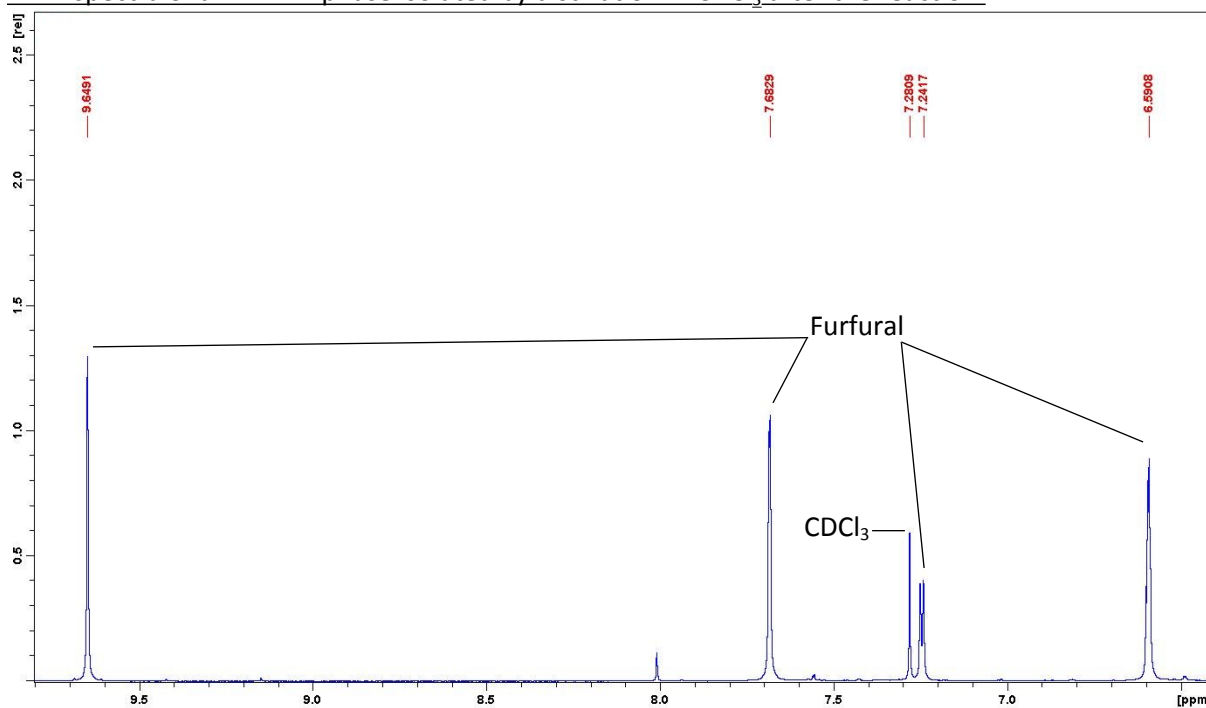
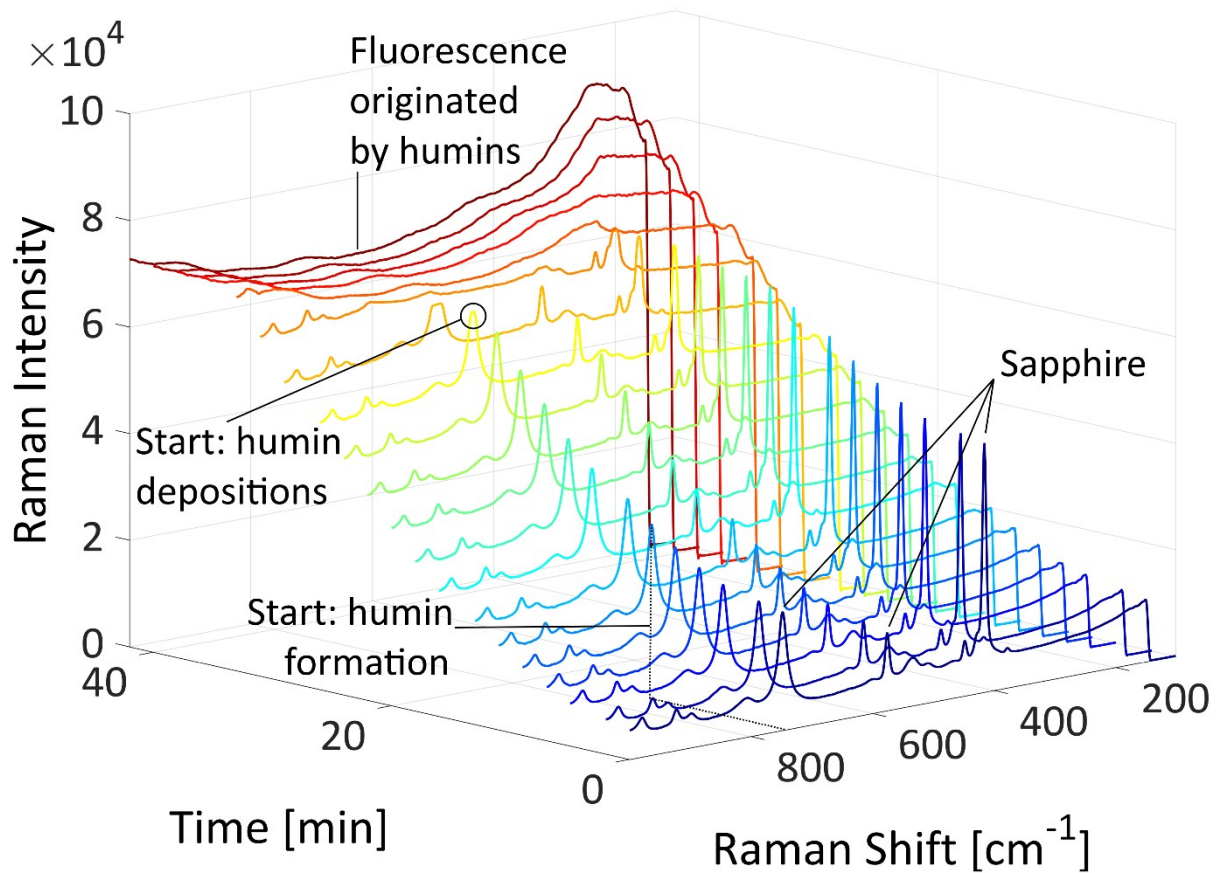


Figure 8:  $^1\text{H}$  NMR spectrum of a xylose dehydration to furfural at  $T = 140^{\circ}\text{C}$  ( $t = 4$  h) measured with AV-400 from Bruker at room temperature ( $^1\text{H}$ -NMR (400 MHz,  $[\text{D}_1]$   $\text{CDCl}_3$ ,  $25^{\circ}\text{C}$ , TMS):  $\delta = 9.58$  (s, 1H, -CHO), 7.62 (s, 1H, -CH-), 7.19 (d,  $^2J = 3.6$  Hz, 1H, -CH-) 6.53 (dd,  $^2J = 3.6$  Hz,  $J = 1.7$  Hz, 1H, -CH-) ppm).

#### 4. Raman spectra over the course of the reaction

Figure 9 shows the development of the Raman spectra over the course of the reaction. At the beginning of the reaction, the signal of the sapphire at  $748\text{ cm}^{-1}$  did not vary (dark blue) because sapphire was an inert material under the reaction conditions. Subsequently, the baseline under the sapphire peak at  $748\text{ cm}^{-1}$  exhibited a strong (light blue to green) increase due to fluorescence originated by the start of humin production. The fluorescence increased and the baseline under the sapphire peak increased to the detection limit of the Raman spectrometer (yellow to red) because of the beginning of humin depositions on the surface of the optical probes and the sapphire peak at  $748\text{ cm}^{-1}$  vanished.



**Figure 9:** Raman spectra between  $200 - 900\text{ cm}^{-1}$  over the course of the reaction ( $T:150\text{ }^\circ\text{C}$ , colour: increase in reaction time).

## 5. Chemometric peak integration models

Peak integration model for ATR mid-IR spectra:

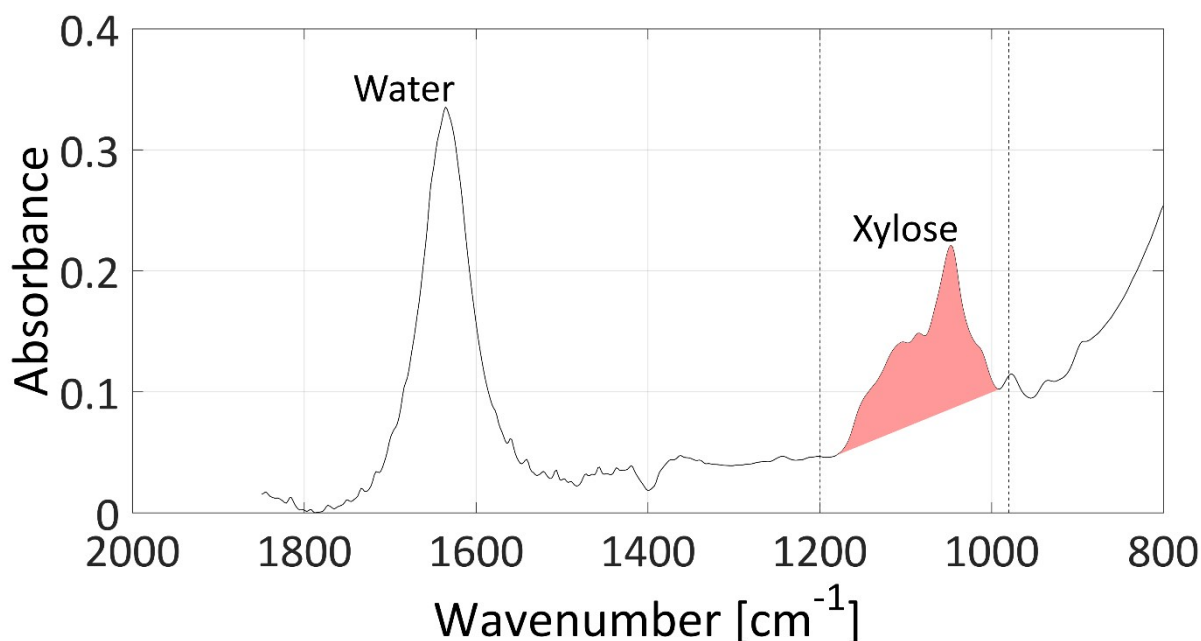


**Figure 10:** Integral of the xylose peak in the mid-IR region between  $980\text{ cm}^{-1}$  –  $1200\text{ cm}^{-1}$  with a linear fit baseline correction (spectrum:  $T$ :  $150\text{ }^{\circ}\text{C}$ ,  $t$ :  $0\text{ s}$ ,  $c_{0, \text{xylose}}$ :  $1.1\text{ mol L}^{-1}$ ).

**Table 3:** Data used for the calibration of the PI model for quantitative xylose analysis. All samples have been prepared gravimetrically and measured at room temperature.

#	$m(\text{H}_2\text{O})$ /mg	$m(\text{Xylose})$ /mg	$m(\text{FeSO}_4 \times 7 \text{H}_2\text{O})$ /mg	$c(\text{Xylose})$ /mol L <sup>-1</sup>
1	1984.7	122.3	73.9	0.387
2	1982.7	180.8	72.6	0.562
3	1997.2	240.4	74.3	0.718 <sup>a</sup>
4	1995.9	270.2	74.3	0.794 <sup>b</sup>
5	1989.4	300.0	73.6	0.897 <sup>c</sup>
6	1998.1	330.2	74.9	0.967
7	2005.2	359.3	72.6	1.048
8	1988.3	368.9	75.2	1.081
9	2003.4	427.7	77.3	1.224
10	1947.0	421.3	76.0	1.238
11	2002.2	484.0	75.7	1.364

<sup>a,b,c</sup>: with 38.5 mg, 57.6 mg, 20.0 mg furfural, respectively

**Table 4:** Data used for the validation of the PI model for quantitative xylose analysis. The true concentration was determined by HPLC from samples of the reaction mixture taken at the end of a reaction and compared to the PI evaluation of the inline data of the respective spectrum.

#	True $c(\text{Xylose})$ /mol L <sup>-1</sup>	Pred. $c(\text{Xylose})$ /mol L <sup>-1</sup>	$\Delta c(\text{Xylose})$ /mol L <sup>-1</sup>
1	0.732	0.709	-0.0229
2	0.826	0.771	-0.0550
3	0.868	0.868	-0.0008

Peak integration models for Raman spectra:

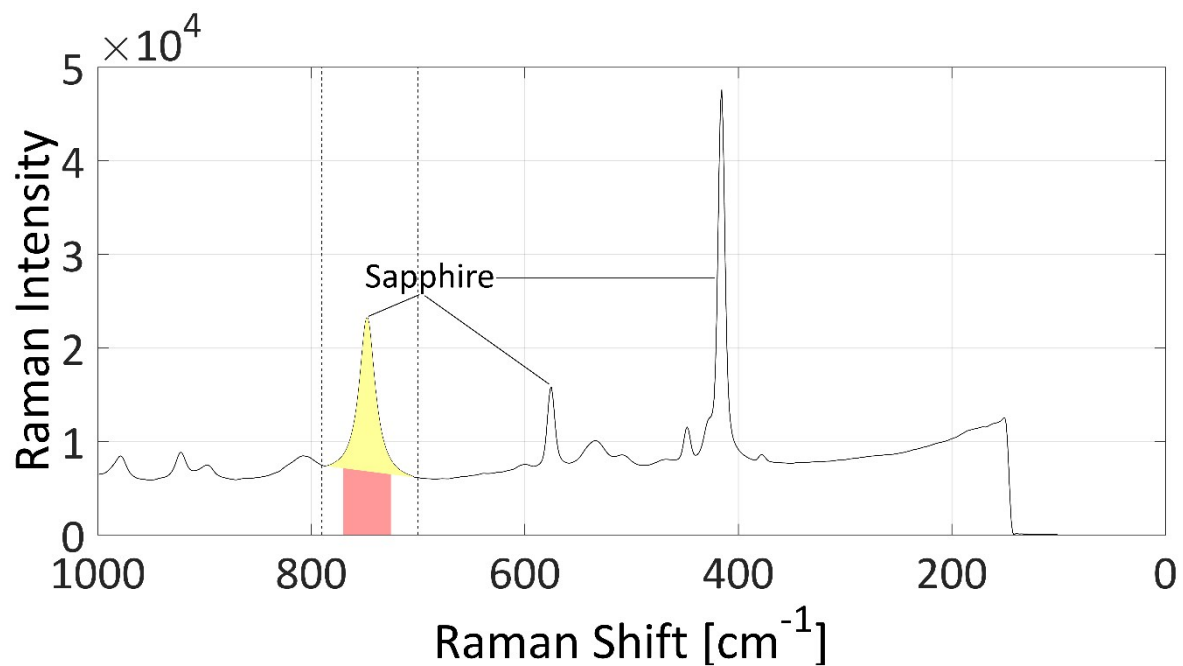


**Figure 11:** Integral of sapphire peak in the Raman region between  $725 \text{ cm}^{-1}$  –  $770 \text{ cm}^{-1}$  with (yellow) and without (red) linear fit baseline correction. Non-marked peaks originated by xylose (spectrum:  $T$ :  $150 \text{ }^\circ\text{C}$ ,  $t$ :  $0 \text{ s}$ ,  $c_{0, \text{xylose}}$ :  $1.1 \text{ mol L}^{-1}$ ).

## 6. Sensitivity analysis

The confidence in the kinetic model strongly depends on the error of the kinetic fitting together with the sensitivity of the fit towards variances in the input variables. The output variable of the kinetic modelling was the activation energy with a value of  $E_A = 151 \text{ kJ mol}^{-1}$  for the dehydration of xylose with an error of the kinetic fitting according to the Arrhenius equation of  $\pm 3 \text{ kJ mol}^{-1}$ . The input variable, the reaction rate constant  $k$  for the different temperatures, was determined by fitting first order kinetics to the inline data with insignificant deviations. However, due to additional experimental source of errors, the mean value of the reaction rate constant (determined seven times) at  $140 \text{ }^\circ\text{C}$  was  $4.93 \cdot 10^{-5} \text{ kJ mol}^{-1}$  with a variance of  $\pm 7.76 \%$ .

To show the influence of the experimental error of the determination of the reaction rate constant on the activation energy, the kinetic modelling of the activation energy according to the Arrhenius equation was performed 5000 times with MATLAB R2015b. Each time, the reaction rate constants for every temperature used for the fitting were allowed to deviate from the experimentally determined values with a random variance between  $-7.76 \%$  and  $+7.76 \%$ . The scatter plot in Figure 12 shows the activation energy of a specific kinetic modelling plotted against the mean deviation of the reaction rate constant used for that fit.

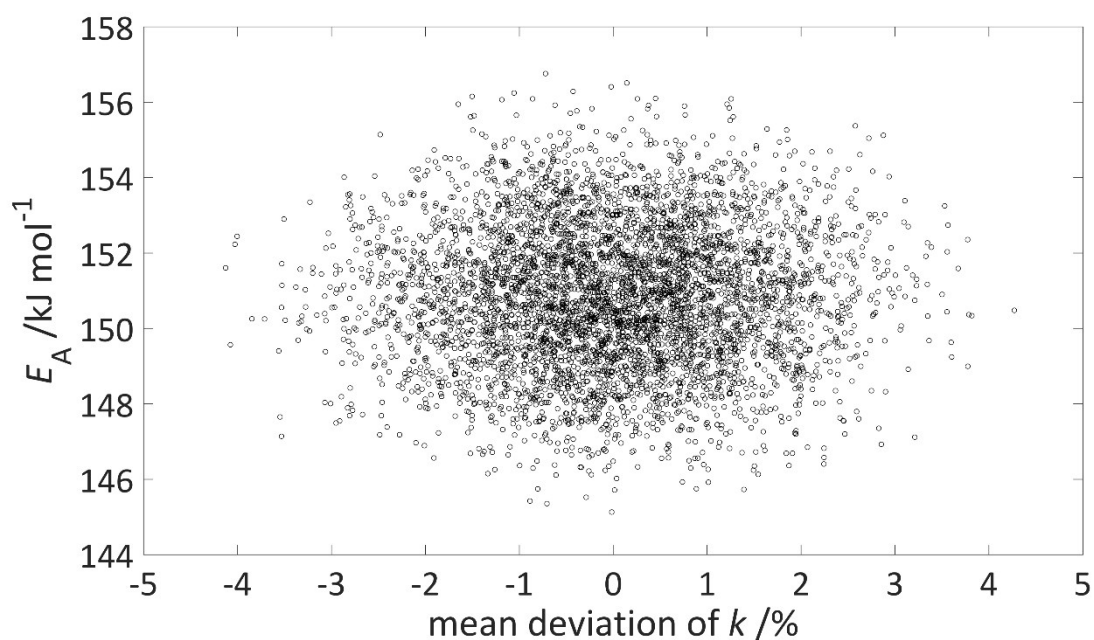


**Figure 12:** Scatter plot of the sensitivity analysis on the influence of the variance of the reaction rate constant on the modelled activation energy.

The scatter plot shows that the modelling of the activation energy was only slightly sensitive to variances in the reaction rate constants, with most values of  $E_A$  ranging between  $148 - 154 \text{ kJ mol}^{-1}$ . This range of  $E_A$  resembled exactly the error of the kinetic fitting according to the Arrhenius equation of  $\pm 3 \text{ kJ mol}^{-1}$ .

The unlikely but strongest influence of the variances of the experimentally determined reaction rate constants on the modelling of  $E_A$  can be seen in the scatter plot and is shown in Figure 13 with a resulting activation energy of  $145 \pm 3 \text{ kJ mol}^{-1}$  or  $156 \pm 3 \text{ kJ mol}^{-1}$ . The deviation of the reaction rate constant varied symmetrically around the temperature of  $140 \text{ }^\circ\text{C}$  which led to the highest shift of the slope in the Arrhenius plot. Although this difference was unlikely to occur within our experimental

measurements, we were able to deduce from the sensitivity analysis that in the event of the highest variances of  $k$  on  $E_A$  the error margins of the kinetic modelling would overlap with each other.

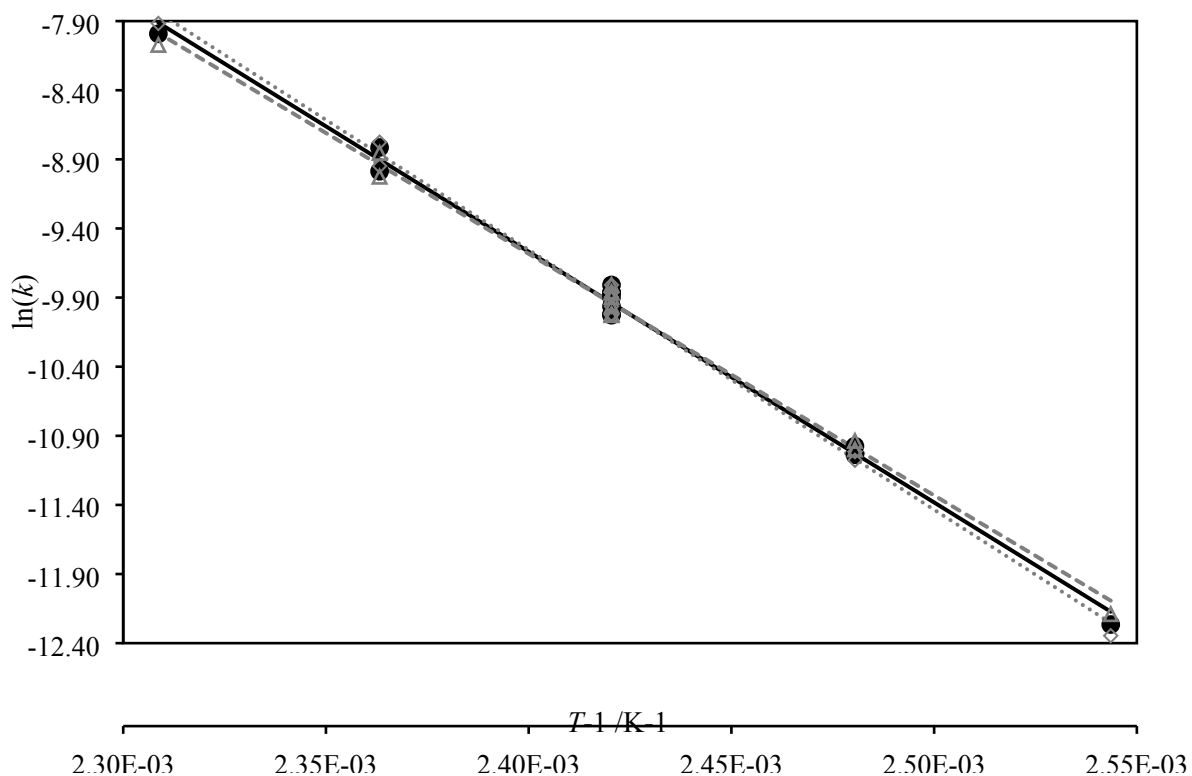


**Figure 13:** Arrhenius diagram for the dehydration of xylose to furfural (black line) together with the strongest influence of variances of the experimentally determined reaction rate constants on this modelling (dashed and dotted grey line).